JACS
JOURNAL OF THE AMERICAN CHEMICAL SOCIETY

Article

pubs.acs.org/JACS

Rigid, Conjugated Macrocycles for High Performance Organic Photodetectors

Boyuan Zhang, M. Tuan Trinh, Brandon Fowler, Melissa Ball, Qizhi Xu, Fay Ng, Michael L. Steigerwald, X.-Y. Zhu,* Colin Nuckolls,* and Yu Zhong*

Department of Chemistry, Columbia University, New York, New York 10027, United States

Supporting Information

ABSTRACT: Organic photodetectors (OPDs) are attractive for their high optical absorption coefficient, broad wavelength tunability, and compatibility with lightweight and flexible devices. Here we describe a new molecular design that enables high performance organic photodetectors. We use a rigid, conjugated macrocycle as the electron acceptor in devices to obtain high photocurrent and low dark current. We make a direct comparison between the devices made with the macrocyclic acceptor and an acyclic control molecule; we find that the superior performance of the macrocycle originates from its rigid, conjugated, and cyclic structure. The macrocycle's rigid structure reduces the number of charged defects originating from deformed sp^2 carbons and covalent defects from photo/thermoactivation. With this molecular design, we are able to suppress dark current density while retaining high responsivity in an ultrasensitive nonfullerene OPD. Importantly, we achieve a detectivity of ~10^{14} Jones at near zero bias voltage. This is without the need for extra carrier blocking layers commonly employed in fullerene-based devices. Our devices are comparable to the best fullerene-based photodetectors, and the sensitivity at low working voltages (<0.1 V) is a record for nonfullerene OPDs.

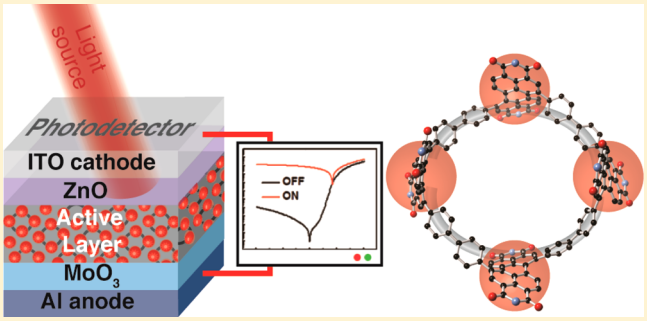

INTRODUCTION

In this Article, we describe a new molecular design for creating organic photodetectors (OPDs) with unparalleled ability to detect photons. The use of organic materials as the active component in photodetectors is attractive because of the potential ease of their fabrication as lightweight and mechanically flexible devices.[1−4] One critical parameter that limits OPD performance is high dark current, because it determines the noise current level and sensitivity of an OPD. The state-of-the-art for OPDs employs a number of modifications such as carrier blocking layers,[5] vertical phase separation,[6] and thick active layers,[7] to lower the dark current. An alternative approach is to use reaction chemistry to build the desired properties into the structure of the active molecule to minimize the intrinsic charge carriers in the active layers.

The dark current in organic, electronic materials is multifaceted, and its origins are not completely understood. Previous studies suggest that the intrinsic conductivity of organic semiconductors is dominated by the intrinsic free carriers, which are usually generated from charged defects.[11] For example, covalent defects formed upon photo/thermoactivation[8−10] and mechanically deformed sp^2 carbon−carbon bonds in π-conjugated molecules are known to produce charged defects that introduce carriers.[11−14] Fullerenes, which are one of the most ubiquitous organic electronic materials, undergo a facile dimerization when irradiated. The dimerization process, however, may yield radicals that produce free carriers.[8,9] This also contributes to the dark current.[11]

To address these issues, we designed a macrocycle that consists of redox-active diphenyl perylenediimide (**P**) wrapped into a tetrameric structure (Figure 1A). We call this $\mathbf{cP_4}$. We find that when we incorporate $\mathbf{cP_4}$ into OPDs the devices have high sensitivity for visible light detection in a very simple device structure. The macrocycle contains several key design elements to yield the highly sensitive OPD result: (1) the rigid structure, constrained in a ring, minimizes the number of charged defects originated from deformed sp^2 carbons; (2) no covalent defects are formed upon photo/thermoactivation; (3) it is efficacious at transporting electrons; (4) and it has high visible light absorption that yields significant photocurrent in a bulk heterojunction photodiode.[15] Using this design we are able to suppress the dark current density while retaining high responsivity in an ultrasensitive nonfullerene OPD. Without the need for extra carrier blocking layers, the highest detectivity in our device approaches 10^{14} Jones at near zero bias voltage. This detectivity is comparable to the best fullerene-based photodetectors, and the sensitivity at low working voltages (<0.1 V) is a record for nonfullerene OPDs. A direct comparison between $\mathbf{cP_4}$ and an acyclic control molecule

Received: September 30, 2016
Published: December 12, 2016

DOI: 10.1021/jacs.6b10276
J. Am. Chem. Soc. 2016, 138, 16426−16431

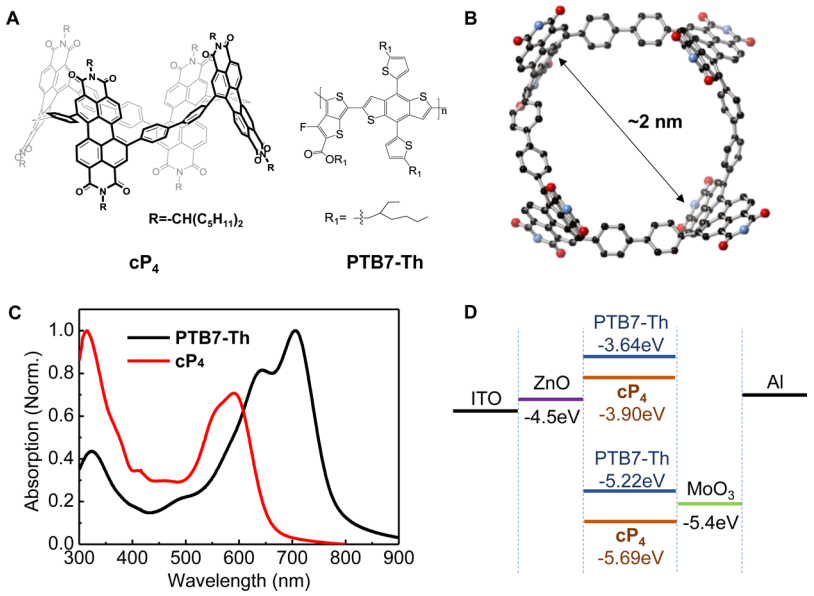

Figure 1. (A) Molecular structure of $\mathbf{cP_4}$ and PTB7-Th. (B) Energy minimized structures from DFT for $\mathbf{cP_4}$. Carbon = gray, nitrogen = blue, oxygen = red. Hydrogen atoms have been removed to clarify the view. A methyl group substitutes the side chains in the calculations. The methyl group, too, has been removed to clarify the view in the structures presented here. (C) Normalized film absorption spectra of PTB7-Th and $\mathbf{cP_4}$. (D) Schematic of the energy levels of ITO, ZnO, PTB7-Th, $\mathbf{cP_4}$, MoO_3, and Al. Energy levels of PTB7-Th and $\mathbf{cP_4}$ were estimated from cyclic voltammetry measurements in solution and adopted from refs 18 and 15, respectively.

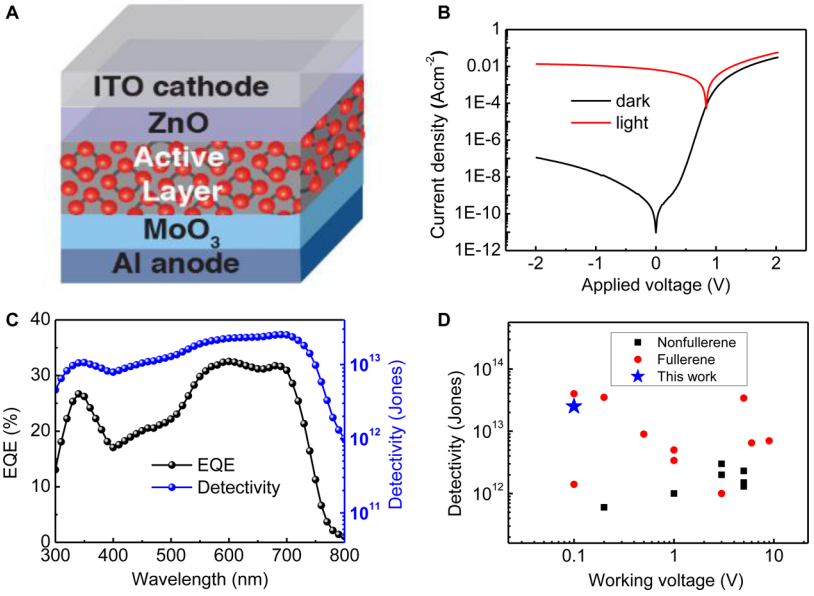

Figure 2. (A) Device structure for the inverted organic photodetector. (B) Current density−voltage curves under dark condition and simulated AM 1.5 G irradiation (100 mW cm^{-2}). (C) External quantum efficiency and specific detectivity spectra calculated at −0.1 V bias voltage. (D) Comparison of detectivity and working voltage in reported organic photodetectors and this work.[5,7,19−32]

reveals that $\mathbf{cP_4}$'s superior performance originates from its rigid, conjugated, and macrocyclic structure.

RESULTS AND DISCUSSION

In a previous study, we found that $\mathbf{cP_4}$ is an n-type semiconductor that transports electrons in both field effect transistors and solar cells.[15] Figure 1B shows $\mathbf{cP_4}$'s energy minimized structure, according to density functional theory (DFT). $\mathbf{cP_4}$'s ∼2 nm diameter cavity in its interior is large enough to thread donor polymers (Figure 1B); its branched side chains impart high solubility in common organic solvents. In solution, the lowest-energy absorption peak at 585 nm has an extinction coefficient of 7.9×10^4 M^{-1} cm^{-1} (Figure S1). The active layer of the photodetector is a blended film of $\mathbf{cP_4}$ and the commercially available polymer donor PTB7-Th (Figure 1A).[16,17] The absorption of PTB7-Th is bathochromically shifted relative to $\mathbf{cP_4}$ (Figure 1C). Figure 1D contains the energy diagram of the materials used in this device. We note the energy offset between the donor's lowest unoccupied molecular orbital (LUMO) and the acceptor's LUMO is well-matched (Figure 1D); energy levels were estimated from cyclic voltammetry (CV).[15,18]

Figure 2A shows a model of a simple device structure that was used in this study. The thickness of the active film is ∼150

DOI: 10.1021/jacs.6b10276
J. Am. Chem. Soc. 2016, 138, 16426−16431

Table 1. Summary of OPD Device Parameters Measured at −0.1 V Bias Voltage

	J_d (A cm^{-2})	EQE (%)	R (AW^{-1})	D^* (Jones)
cP$_4$	1.5×10^{-10}	33 @600 nm	0.18 @690 nm	2.5×10^{13} @690 nm
$PC_{71}BM$	5.6×10^{-7}	70 @640 nm	0.39 @710 nm	9.2×10^{11} @710 nm
aP$_n$	1.0×10^{-9}	22 @350 nm	0.09 @680 nm	4.8×10^{12} @680 nm

nm. Figure 2B displays the current−voltage curves for a typical OPD under dark conditions and simulated AM 1.5G irradiation (100 mW cm^{-2}). One of the exciting findings is that the OPD possesses extremely small dark current at reverse bias voltage. The dark J−V curve shows a high rectification ratio of >10^5 at ±2 V and a dark current density as small as 1.4×10^{-10} A cm^{-2} at −0.1 V. This dark current density is 1 order of magnitude lower than the best fullerene-free OPDs[7] and comparable with fullerene-based OPDs and perovskite photodetectors.[5,33] Notably, both fullerene-based OPDs and perovskite photodetectors need extra electron or hole blocking layers in order to achieve a low level of the dark current.[5,33] Equally important is the large photocurrent that is generated upon photoexcitation at small reverse bias voltages. The on/off ratio is >10^7 calculated at −0.1 V under simulated AM 1.5G irradiation (100 mW cm^{-2}). The OPD device described here can operate at small bias voltages and even at zero bias. This compares favorably with previously reported nonfullerene OPDs; they require much larger reverse bias voltages (typically −1 to −3 V) to operate due to the poor carrier extraction.[22−25,30]

Ultralow dark current could result from poor carrier transport ability. This is not the case for **cP$_4$**. As discussed above, **cP$_4$** effectively transports electrons generated upon photoexcitation. This allows the OPD to operate at a small bias voltage. We inherently achieve high photocurrent and low dark current simultaneously in the **cP$_4$** OPD with a thin active layer and a simple device structure. **cP$_4$** is an ideal design for an electron acceptor to create a highly sensitive nonfullerene OPD.

Table 1 summarizes the responsivity (R), specific detectivity (D^*), external quantum efficiency (EQE) and dark current density (J_d) for the OPD device data for the PTB7-Th:**cP$_4$** blended films. The devices have a linear dynamic range (LDR) > 140 dB (Figure S2) and cutoff frequency of 467 kHz (Figure S3). Overall the device characteristics are excellent; in particular, **cP$_4$** greatly excels in detectivity. We find that the specific detectivity is more than 10^{13} Jones over the whole visible light region at −0.1 V. The highest D^* was calculated to be 2.5×10^{13} Jones at 700 nm (Figure 2C). At zero bias, the calculated specific detectivity is as high as 1×10^{14} Jones. These values are among the highest detectivities for the state-of-the-art fullerene photodetector[5,19−22,26−29,32] and much higher than the best nonfullerene OPDs[7,23−25,30,31,34] (Figure 2D). Moreover, the **cP$_4$**-based OPD requires much smaller working voltage compared with other nonfullerene OPDs because of their relatively high responsivity (R) near zero bias voltage (Figure 2D).

One of the two key parameters responsible for high responsivity (R) is efficient charge generation from photoexcitation in the active layer. Extensive research on molecular donor/acceptor interfaces has pointed to the critical role of electronic delocalization in facilitating efficient charge separation at the donor/acceptor interfaces.[35,36] In particular, the spherical fullerene based electron acceptors are believed to transport charge efficiently due to their three-dimensional connectivity in ensuring electronic delocalization on the acceptor side.[37,38] Can **cP$_4$** provide similar connectivity and electronic delocalization that is necessary for charge separation? While the high responsivity near zero bias suggests the answer above is affirmative, we further support this by studying the efficient charge separation at the PTB7-Th/**cP$_4$** interface using transient absorption (TA) spectroscopy (see the Supporting Information for the details of the experiment).

The linear absorption spectra in Figure 1C show that the donor material, PTB7-Th can be selectively excited at 710 nm in the blended film; subsequently, we can monitor electron transfer from PTB7-Th to **cP$_4$**. At a short pump−probe delay (0.25 ps), we observe features arising from PTB7-Th (red curve in Figure 3A) with the bleaching at 630 and 715 nm and excited

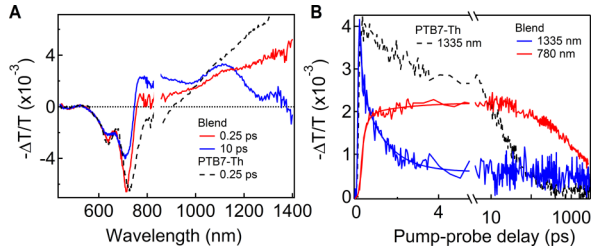

Figure 3. Transient absorption spectra (A) and dynamics (B) for the neat film of PTB7-Th and blended film of **cP$_4$** and PTB7-Th pumped at 710 nm. The dashed black curves are from PTB7-Th which were scaled for comparison.

state absorption (ESA) in the near IR range. This is similar to the TA spectrum from the neat PTB7-Th film (black dashed curve in Figure 3A). The bleaching in PTB7-Th is reduced and new ESA transitions from 770 to 1300 nm evolve as the delay time increases. These new ESA features centered at 840 and 1120 nm are attributed to the charge (polaron) absorptions in the perylenediimide (PDI) and PTB7-Th moieties, respectively.[39−41] While the ESA of the PTB7-Th singlet dominates in the long probe wavelength range (>1300 nm), the ESA of charges in either donor or acceptor materials is negligible. Thus, dynamics at 1335 nm are a good measure of exciton dissociation at the donor/acceptor interface. Figure 3B shows that the biexponential fit (blue curve) to the dynamics at 1335 nm (blue dots) yields time constants of 0.11 ± 0.04 ps (42% weight) and 1.2 ± 0.1 ps (58% weight). The charge buildup monitored by polaron ESA at 780 nm (red dots) gives nearly identical time constants (red curve). These time constants indicate ultrafast electron transfer from PTB7-Th to **cP$_4$**. The short time constant can be attributed to the instantaneous charge transfer near the interface upon photoexcitation, while the longer time constant is attributed to exciton diffusion in PTB7-Th prior to the dissociation event.[40,41] For comparison, the singlet exciton lifetime in neat PTB7-Th is of the order of nanoseconds (black dashed curve in Figure 3B). This is much longer than that in the blend. We also observe similarly ultrafast hole transfer from **cP$_4$** to PTB7-Th when both donor and acceptor are excited at 560 nm (see the Supporting Information). These measurements confirm that **cP$_4$** photo-

DOI: 10.1021/jacs.6b10276
J. Am. Chem. Soc. 2016, 138, 16426−16431

detector performance is comparable, if not better than that of a fullerene, for exciton dissociation in blend films.[42−45]

The second important parameter that determines the high detectivity in these devices is the dark current density. To gain insight into the origin of the device characteristics, we analyze the $J-V$ curve under dark conditions to calculate the reverse saturation dark current J_0. The fitting method is detailed in the Supporting Information. The saturation dark current density is as low as 7.7×10^{-13} A cm^{-2} (Figure S5). The intrinsic conductivity is determined by the intrinsic free carrier density and the mobility. Photocurrent and thin film field effect transistor measurements reveal efficacious electron transporting ability.[15] Therefore, such a low level of J_0 indicates a small amount of intrinsic free carrier density. To verify that the intrinsic conductivity of the thin films is dominated by the charged defects, we measured the dependence of the dark current density on temperature. The activation energies are calculated to be (0.15 ± 0.01) eV and (0.20 ± 0.01) eV at -2 V and -0.5 V, respectively (Figure S6). These values are much smaller than the band gaps of the active organic components (Figure 1D) and are consistent with thermal activation energy of locally bound charged defects.[11,46]

To better understand the origin of the low density of charged defects in **cP$_4$**, we made a direct comparison between a PC$_{71}$BM and a **cP$_4$** based OPD with the same device structure as shown in Figure 2A. Although the responsivity (R) of the PC$_{71}$BM-based OPD is approximately 2-fold higher than that of the **cP$_4$**-based device (Table 1 and Figure S8), the dark current of the PC$_{71}$BM-based device is 2−3 orders of magnitude higher than that of the **cP$_4$**-based one (Figure 4B). It is obvious that the dark current level dominates the detectivity in this type of OPD. Thus, the detectivity of the **cP$_4$**-based OPD is more than 1 order of magnitude higher than that of the PC$_{71}$BM-based one (Figure 4C). One of the origins of the high dark current is from the chemistry of fullerenes. PC$_{71}$BM is known to undergo dimerization that is initiated by electron donors, metals, and photons.[8−10,47,48] In each of these cases, in a solid state film, the partners need to be unencumbered and in the correct orientation for the reaction to occur. In the absence of these conditions, the films will contain carriers that contribute to the relatively high dark current.[8−10] Fullerene-based OPDs require extra blocking layers to minimize this relatively high dark current. Compared with fullerenes, PDIs are known to exhibit exceptional chemical, thermal and photochemical stability.[49−53] They have also been widely used as building blocks to construct macrocycles.[54−65] The PDI units in **cP$_4$** have no easily accessible pathway to introduce these same type of covalent defects. This accounts for the low intrinsic conductivity in **cP$_4$** OPDs.[11]

In order to assess the importance of the cyclic, rigid structure of **cP$_4$**, we synthesized an acyclic, polymeric version, named, **aP$_n$** (Figure 4A). Overall, the **aP$_n$** photodetector performs very well and shows high sensitivity. Although the responsivity of the **aP$_n$** OPD is about one-fourth of that in the PC$_{71}$BM OPD, the dark current density in the **aP$_n$** OPD is 1 order of magnitude lower than that in the PC$_{71}$BM OPD (Figure 4B). As a result, the **aP$_n$** OPD shows a doubling of the detectivity compared to the PC$_{71}$BM OPD (Figure 4C). These results, once again, suggest that dark current dominates the sensitivity and confirm the importance of incorporating chemically stable PDIs into electron acceptors in OPDs. Even so, the **aP$_n$** OPD is still not as effective as the **cP$_4$** OPD in terms of detectivity. As a comparison, the **aP$_n$**-based OPD has a dark current 1.0×10^{-9} A cm^{-2} at -0.1 V, which is about 10-fold higher than that of the **cP$_4$**-based device (see Table 1 and Figure 4B). In addition, the **aP$_n$**-based OPD also shows lower responsivity compared to **cP$_4$** devices (Table 1 and Figure S8). The resulting peak D^* for the **aP$_n$**-based OPD is 4.8×10^{12} Jones at 680 nm, only about one-third of the peak value in the **cP$_4$**-based OPD. This is because intrinsic, charged defects in linear polymer semiconductors originate from end groups[13,66,67] and deformed sp^2 carbons near the rotatable C−C single bonds.[11−14] The torsional effect is inevitable in linear molecules with flexible backbones. These problems are eliminated by winding linear molecules into rigid, conjugated macrocycles with no end groups.[15,68] The macrocyclic **cP$_4$** possesses a locked conformation with higher rigidity (Figure 1B) and is expected to create fewer locally charged defects relative to the linear polymeric counterpart.

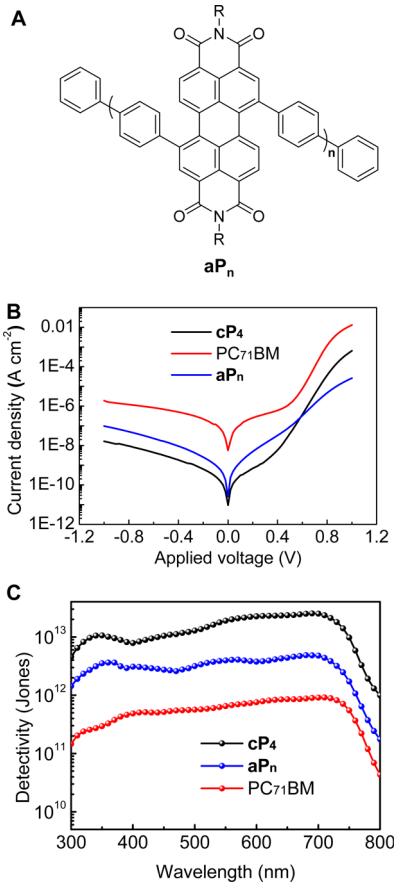

Figure 4. (A) Molecular structure of **aP$_n$** used to test the origin of the low dark current. (B) Dark current density−voltage curves for PC$_{71}$BM, **aP$_n$**, and **cP$_4$** based photodetectors with the same device structure as shown in Figure 2A. (C) Specific detectivity spectra for **cP$_4$**, **aP$_n$**, and PC$_{71}$BM based OPDs calculated at -0.1 V bias voltage.

CONCLUSION

The results described above show that the rigid, cyclic molecular structure is an important design criterion to achieve ultralow intrinsic conductivity in the OPDs. We found that the rigid, conjugated macrocycle is able to act as the electron acceptor in high performance OPDs. Using this molecular design, we are able to suppress dark current density while retaining high responsivity in an ultrasensitive nonfullerene OPD. Without the need for extra carrier blocking layers, this detectivity is comparable to the best fullerene-based photo-

DOI: 10.1021/jacs.6b10276
J. Am. Chem. Soc. 2016, 138, 16426−16431

detectors, and the sensitivity at low working voltages is a record for nonfullerene OPDs. It is clear from this study that the devices can be further improved by designing the electron donating material to form a shape and electronic match for these macrocyclic electron acceptors.

■ ASSOCIATED CONTENT

Supporting Information

The Supporting Information is available free of charge on the ACS Publications website at DOI: 10.1021/jacs.6b10276.

Device fabrication, characterization methods, UV−vis spectroscopy, linear dynamic range (LDR) measurement, frequency-dependent measurement, transient absorption (TA) spectra, dark current−voltage characteristics, temperature-dependent dark current measurement, device performance (PDF)

■ AUTHOR INFORMATION

Corresponding Authors

*xz2324@columbia.edu
*cn37@columbia.edu
*yz2435@columbia.edu

ORCID

X.-Y. Zhu: 0000-0002-2090-8484
Colin Nuckolls: 0000-0002-0384-5493

Notes

The authors declare no competing financial interest.

■ ACKNOWLEDGMENTS

C.N. thanks Sheldon and Dorothea Buckler for their generous support. Primary support for this project was provided by the Chemical Sciences, Geosciences and Biosciences Division, Office of Basic Energy Sciences, U.S. Department of Energy (DOE), under Award No. DE-FG02-01ER15264. X-Y.Z. and C.N. acknowledge support from U.S. Department of Energy (DOE), under Award No. DE-SC0014563 for transient absorption experiments. Research was carried out in part at the Center for Functional Nanomaterials, which is a U.S. DOE Office of Science Facility, at Brookhaven National Laboratory under Contract No. DE-SC0012704. We thank Dr. Sfeir for help with the transient absorption setup. The Columbia University Shared Materials Characterization Laboratory (SMCL) was used extensively for this research. We are grateful to Columbia University for support of this facility.

■ REFERENCES

(1) Baeg, K.-J.; Binda, M.; Natali, D.; Caironi, M.; Noh, Y.-Y. *Adv. Mater.* **2013**, *25*, 4267.
(2) Sekitani, T.; Noguchi, Y.; Hata, K.; Fukushima, T.; Aida, T.; Someya, T. *Science* **2008**, *321*, 1468.
(3) Rogers, J. A.; Someya, T.; Huang, Y. G. *Science* **2010**, *327*, 1603.
(4) Ball, M.; Zhong, Y.; Wu, Y.; Schenck, C.; Ng, F.; Steigerwald, M.; Xiao, S.; Nuckolls, C. *Acc. Chem. Res.* **2015**, *48*, 267.
(5) Gong, X.; Tong, M.; Xia, Y.; Cai, W.; Moon, J. S.; Cao, Y.; Yu, G.; Shieh, C.-L.; Nilsson, B.; Heeger, A. J. *Science* **2009**, *325*, 1665.
(6) Zhang, L.; Yang, T.; Shen, L.; Fang, Y.; Dang, L.; Zhou, N.; Guo, X.; Hong, Z.; Yang, Y.; Wu, H.; Huang, J.; Liang, Y. *Adv. Mater.* **2015**, *27*, 6496.
(7) Kim, I. K.; Li, X.; Ullah, M.; Shaw, P. E.; Wawrzinek, R.; Namdas, E. B.; Lo, S. C. *Adv. Mater.* **2015**, *27*, 6390.
(8) Segura, J. L.; Martin, N. *Chem. Soc. Rev.* **2000**, *29*, 13.
(9) Tsetseris, L.; Pantelides, S. T. *Phys. Rev. B: Condens. Matter Mater. Phys.* **2011**, *84*, 195202.
(10) Sheka, E. F. *Chem. Phys. Lett.* **2007**, *438*, 119.
(11) Gregg, B. A. *Soft Matter* **2009**, *5*, 2985.
(12) Darling, S. B. *J. Phys. Chem. B* **2008**, *112*, 8891.
(13) Kaake, L. G.; Barbara, P. F.; Zhu, X. Y. *J. Phys. Chem. Lett.* **2010**, *1*, 628.
(14) Gregg, B. A.; Chen, S.-G.; Cormier, R. A. *Chem. Mater.* **2004**, *16*, 4586.
(15) Ball, M.; Zhong, Y.; Fowler, B.; Zhang, B.; Li, P.; Etkin, G.; Paley, D. W.; Decatur, J.; Dalsania, A. K.; Li, H.; Xiao, S.; Ng, F.; Steigerwald, M. L.; Nuckolls, C. *J. Am. Chem. Soc.* **2016**, *138*, 12861.
(16) Liang, Y.; Xu, Z.; Xia, J.; Tsai, S.-T.; Wu, Y.; Li, G.; Ray, C.; Yu, L. *Adv. Mater.* **2010**, *22*, E135.
(17) Li, C.-Z.; Chang, C.-Y.; Zang, Y.; Ju, H.-X.; Chueh, C.-C.; Liang, P.-W.; Cho, N.; Ginger, D. S.; Jen, A. K. Y. *Adv. Mater.* **2014**, *26*, 6262.
(18) Liao, S.-H.; Jhuo, H.-J.; Cheng, Y.-S.; Chen, S.-A. *Adv. Mater.* **2013**, *25*, 4766.
(19) Armin, A.; Hambsch, M.; Kim, I. K.; Burn, P. L.; Meredith, P.; Namdas, E. B. *Laser & Photonics Rev.* **2014**, *8*, 924.
(20) Binda, M.; Iacchetti, A.; Natali, D.; Beverina, L.; Sassi, M.; Sampietro, M. *Appl. Phys. Lett.* **2011**, *98*, 073303.
(21) Fang, Y.; Guo, F.; Xiao, Z.; Huang, J. *Adv. Opt. Mater.* **2014**, *2*, 348.
(22) Kim, I. K.; Pal, B. N.; Ullah, M.; Burn, P. L.; Lo, S.-C.; Meredith, P.; Namdas, E. B. *Adv. Opt. Mater.* **2015**, *3*, 50.
(23) Lee, K.-H.; Leem, D.-S.; Castrucci, J. S.; Park, K.-B.; Bulliard, X.; Kim, K.-S.; Jin, Y. W.; Lee, S.; Bender, T. P.; Park, S. Y. *ACS Appl. Mater. Interfaces* **2013**, *5*, 13089.
(24) Leem, D.-S.; Lee, K.-H.; Park, K.-B.; Lim, S.-J.; Kim, K.-S.; Wan Jin, Y.; Lee, S. *Appl. Phys. Lett.* **2013**, *103*, 043305.
(25) Lim, S.-J.; Leem, D.-S.; Park, K.-B.; Kim, K.-S.; Sul, S.; Na, K.; Lee, G. H.; Heo, C.-J.; Lee, K.-H.; Bulliard, X.; Satoh, R.-I.; Yagi, T.; Ro, T.; Im, D.; Jung, J.; Lee, M.; Lee, T.-Y.; Han, M. G.; Jin, Y. W.; Lee, S. *Sci. Rep.* **2015**, *5*, 7708.
(26) Pierre, A.; Deckman, I.; Lechêne, P. B.; Arias, A. C. *Adv. Mater.* **2015**, *27*, 6411.
(27) Qi, J.; Zhou, X.; Yang, D.; Qiao, W.; Ma, D.; Wang, Z. Y. *Adv. Funct. Mater.* **2014**, *24*, 7605.
(28) Ramuz, M.; Bürgi, L.; Winnewisser, C.; Seitz, P. *Org. Electron.* **2008**, *9*, 369.
(29) Saracco, E.; Bouthinon, B.; Verilhac, J.-M.; Celle, C.; Chevalier, N.; Mariolle, D.; Dhez, O.; Simonato, J.-P. *Adv. Mater.* **2013**, *25*, 6534.
(30) Wang, J. B.; Li, W. L.; Chu, B.; Lee, C. S.; Su, Z. S.; Zhang, G.; Wu, S. H.; Yan, F. *Org. Electron.* **2011**, *12*, 34.
(31) Wang, X.; Lv, L.; Li, L.; Chen, Y.; Zhang, K.; Chen, H.; Dong, H.; Huang, J.; Shen, G.; Yang, Z.; Huang, H. *Adv. Funct. Mater.* **2016**, *26*, 6306.
(32) Zhang, L.; Yang, T.; Shen, L.; Fang, Y.; Dang, L.; Zhou, N.; Guo, X.; Hong, Z.; Yang, Y.; Wu, H.; Huang, J.; Liang, Y. *Adv. Mater.* **2015**, *27*, 6496.
(33) Dou, L.; Yang, Y.; You, J.; Hong, Z.; Chang, W.-H.; Li, G.; Yang, Y. *Nat. Commun.* **2014**, *5*, 5404.
(34) We do not discuss photomultiplication photodetectors here, as they have different working mechanism and require high work voltages. Examples of photomultiplication photodetectors can be found in: Wang, W.; Zhang, F.; Bai, H.; Li, L.; Gao, M.; Zhang, M.; Zhan, X. *Nanoscale* **2016**, *8*, 5578.
(35) Zhu, X.; Monahan, N. R.; Gong, Z.; Zhu, H.; Williams, K. W.; Nelson, C. A. *J. Am. Chem. Soc.* **2015**, *137*, 8313.
(36) Banerji, N. *J. Mater. Chem. C* **2013**, *1*, 3052.
(37) Savoie, B. M.; Jackson, N. E.; Chen, L. X.; Marks, T. J.; Ratner, M. A. *Acc. Chem. Res.* **2014**, *47*, 3385.
(38) Savoie, B. M.; Rao, A.; Bakulin, A. A.; Gelinas, S.; Movaghar, B.; Friend, R. H.; Marks, T. J.; Ratner, M. A. *J. Am. Chem. Soc.* **2014**, *136*, 2876.
(39) Zhong, Y.; Trinh, M. T.; Chen, R.; Wang, W.; Khlyabich, P. P.; Kumar, B.; Xu, Q.; Nam, C. Y.; Sfeir, M. Y.; Black, C.; Steigerwald, M. L.; Loo, Y. L.; Xiao, S.; Ng, F.; Zhu, X. Y.; Nuckolls, C. *J. Am. Chem. Soc.* **2014**, *136*, 15215.

DOI: 10.1021/jacs.6b10276
J. Am. Chem. Soc. 2016, 138, 16426−16431

(40) Zhong, Y.; Trinh, M. T.; Chen, R.; Purdum, G. E.; Khlyabich, P. P.; Sezen, M.; Oh, S.; Zhu, H.; Fowler, B.; Zhang, B.; Wang, W.; Nam, C. Y.; Sfeir, M. Y.; Black, C. T.; Steigerwald, M. L.; Loo, Y. L.; Ng, F.; Zhu, X. Y.; Nuckolls, C. *Nat. Commun.* **2015**, *6*, 8242.
(41) Kaake, L. G.; Moses, D.; Heeger, A. J. *J. Phys. Chem. Lett.* **2013**, *4*, 2264.
(42) Hwang, I. W.; Soci, C.; Moses, D.; Zhu, Z.; Waller, D.; Gaudiana, R.; Brabec, C. J.; Heeger, A. J. *Adv. Mater.* **2007**, *19*, 2307.
(43) Hwang, I.; Beaupre, S.; Leclerc, M.; Scholes, G. D. *Chem. Sci.* **2012**, *3*, 2270.
(44) Grancini, G.; Maiuri, M.; Fazzi, D.; Petrozza, A.; Egelhaaf, H. J.; Brida, D.; Cerullo, G.; Lanzani, G. *Nat. Mater.* **2013**, *12*, 29.
(45) Gélinas, S.; Rao, A.; Kumar, A.; Smith, S. L.; Chin, A. W.; Clark, J.; van der Poll, T. S.; Bazan, G. C.; Friend, R. H. *Science* **2014**, *343*, 512.
(46) Gregg, B. A. *J. Phys. Chem. C* **2009**, *113*, 5899.
(47) Wang, G.-W.; Komatsu, K.; Murata, Y.; Shiro, M. *Nature* **1997**, *387*, 583.
(48) Komatsu, K.; Wang, G.-W.; Murata, Y.; Tanaka, T.; Fujiwara, K.; Yamamoto, K.; Saunders, M. *J. Org. Chem.* **1998**, *63*, 9358.
(49) Huang, C.; Barlow, S.; Marder, S. R. *J. Org. Chem.* **2011**, *76*, 2386.
(50) Wurthner, F. *Chem. Commun.* **2004**, 1564.
(51) Kozma, E.; Catellani, M. *Dyes Pigm.* **2013**, *98*, 160.
(52) Würthner, F.; Saha-Möller, C. R.; Fimmel, B.; Ogi, S.; Leowanawat, P.; Schmidt, D. *Chem. Rev.* **2016**, *116*, 962.
(53) Zhong, Y.; Kumar, B.; Oh, S.; Trinh, M. T.; Wu, Y.; Elbert, K.; Li, P.; Zhu, X.; Xiao, S.; Ng, F.; Steigerwald, M. L.; Nuckolls, C. *J. Am. Chem. Soc.* **2014**, *136*, 8122.
(54) Langhals, H.; Ismael, R. *Eur. J. Org. Chem.* **1998**, *1998*, 1915.
(55) Wang, W.; Wang, L.; Palmer, B. J.; Exarhos, G. J.; Li, A. D. Q. *J. Am. Chem. Soc.* **2006**, *128*, 11150.
(56) Feng, J.; Zhang, Y.; Zhao, C.; Li, R.; Xu, W.; Li, X.; Jiang, J. *Chem. - Eur. J.* **2008**, *14*, 7000.
(57) Shaller, A. D.; Wang, W.; Gan, H.; Li, A. D. Q. *Angew. Chem., Int. Ed.* **2008**, *47*, 7705.
(58) Wang, W.; Shaller, A. D.; Li, A. D. Q. *J. Am. Chem. Soc.* **2008**, *130*, 8271.
(59) Schlosser, F.; Stepanenko, V.; Wurthner, F. *Chem. Commun.* **2010**, *46*, 8350.
(60) Schlosser, F.; Sung, J.; Kim, P.; Kim, D.; Wurthner, F. *Chem. Sci.* **2012**, *3*, 2778.
(61) Lee, J.-E.; Stepanenko, V.; Yang, J.; Yoo, H.; Schlosser, F.; Bellinger, D.; Engels, B.; Scheblykin, I. G.; Würthner, F.; Kim, D. *ACS Nano* **2013**, *7*, 5064.
(62) Schlosser, F.; Moos, M.; Lambert, C.; Würthner, F. *Adv. Mater.* **2013**, *25*, 410.
(63) Brown, K. E.; Salamant, W. A.; Shoer, L. E.; Young, R. M.; Wasielewski, M. R. *J. Phys. Chem. Lett.* **2014**, *5*, 2588.
(64) Ham, S.; Yang, J.; Schlosser, F.; Würthner, F.; Kim, D. *J. Phys. Chem. Lett.* **2014**, *5*, 2830.
(65) Spenst, P.; Würthner, F. *Angew. Chem.* **2015**, *127*, 10303.
(66) Mandoc, M. M.; de Boer, B.; Paasch, G.; Blom, P. W. M. *Phys. Rev. B: Condens. Matter Mater. Phys.* **2007**, *75*, 193202.
(67) Nicolai, H. T.; Kuik, M.; Wetzelaer, G. A. H.; de Boer, B.; Campbell, C.; Risko, C.; Brédas, J. L.; Blom, P. W. M. *Nat. Mater.* **2012**, *11*, 882.
(68) Ball, M.; Fowler, B.; Li, P.; Joyce, L. A.; Li, F.; Liu, T.; Paley, D.; Zhong, Y.; Li, H.; Xiao, S.; Ng, F.; Steigerwald, M. L.; Nuckolls, C. *J. Am. Chem. Soc.* **2015**, *137*, 9982.

DOI: 10.1021/jacs.6b10276
J. Am. Chem. Soc. 2016, 138, 16426−16431